ADVANCED FUNCTIONAL MATERIALS
www.afm-journal.de

Increase Output Energy and Operation Frequency of a Triboelectric Nanogenerator by Two Grounded Electrodes Approach

*Gang Cheng, Zong-Hong Lin, Zuliang Du, and Zhong Lin Wang**

Triboelectric nanogenerator (TENG) generally operates using two-electrodes to form a closed outer circuit loop without directly contacting ground. Here, a newly designed TENG, the two electrodes of which are grounded for doubling the energy output and the operation frequency, is introduced. The TENG operates in two modes: two-channel mode in which the two electrodes are simultaneously connected to the ground, and single-channel mode in which the two electrodes are alternately connected to the ground through a self-triggered vibrating switch. Both modes doubles the total charges to be transported compared to the traditional ungrounded TENG. For the single-channel TENG, about 30 current peaks with an output frequency of 50 Hz are generated in a single cycle at a motion triggering frequency of 2 Hz. The output energy at a load lower than 10 MΩ of the single-channel TENG is enhanced, and the enhancing ratio is more than 100 at a load of 100 kΩ. The two electrodes grounded TENG provides a new strategy for effective use of the energy harvested from our living environment.

1. Introduction

Harvesting mechanical energy from ambient environment and human body has attracted increasing interest for nano-scale self-powered electronic devices and large-scale energy needs.[1–4] The various physical mechanisms, such as electromagnetic,[5,6] electrostatic,[7,8] and piezoelectric[9–15] effects, have been utilized to harvest mechanical energy. Recently, triboelectric nanogenerator (TENG)[16–28] has been invented as a new technology to harvest mechanical energy, which is based on contact electrification effect and electrostatic induction.[29–31] Various applications of TENG have been demonstrated, such as self-powered chemical sensor,[32,33] electrodegradation,[34] and powering commercial LEDs.[21–25] When two triboelectric surfaces (tribo-surfaces) with opposite triboelectric charges (tribo-charges) are periodically contacted and separated, the potential difference between the metal electrodes of the two tribo-surfaces periodically varies, which drives the free electrons to flow between the two electrodes. The open-circuit voltage of more than 1000 V has been reported for TENG,[21] while, the output voltage decreases with the decrease of the load resistance,[21–25] which should decrease the output power at a lower load resistance. In addition, for providing more continuous power, it is necessary to enhance the output frequency of the TENG. The TENGs operated at rotation disk mode[25] and cylindrical rotation mode[22] have been developed to generate electrical output with a frequency up to several tens of Hertz by harvesting the mechanical energy with high motion frequency. While, when the TENG is driven by mechanical motion with low frequency, how to provide electrical output with high frequency is still an open question. Therefore, it is necessary to investigate the novel operating modes to enhance the output performances of the TENG.

For traditional TENG, the two electrodes of the tribo-surfaces are connected together, the charges flow between the two electrodes, and both electrodes are not grounded,[16–26] which is defined as ungrounded TENG. Recently, a single-electrode-based TENG has been developed,[27,28] in which one electrode is grounded and the charges flow between this electrode and the ground. In this paper, a two-electrode grounded (TEG)-TENG has been developed to enhance the output performance of the TENG. Two modes of the TEG-TENG are demonstrated: two-channel mode and single-channel mode. For single-channel TEG-TENG with self-triggered vibrating switch, about 30 current peaks with an output frequency of 50 Hz are generated in a single cycle as the motion triggering frequency being 2 Hz, and the output energy at a load of 100 kΩ is enhanced for more than 100 times compared to the traditional TENG. This study demonstrates another form of TENG for practical applications.

2. Results and Discussion

The TENGs operate in the typical vertical contact-separation mode,[21] and the structure of the TENG is shown in **Figure 1**a. For the top plate, a square plastic resin (PR) sheet

Dr. G. Cheng, Dr. Z.-H. Lin, Prof. Z. L. Wang
School of Material Science and Engineering
Georgia Institute of Technology
Atlanta, GA 30332–0245, USA
E-mail: zlwang@gatech.edu
Dr. G. Cheng, Prof. Z. L. Du
Key Lab for Special Functional Materials
Henan University
Kaifeng, 475004, China
Prof. Z. L. Wang
Satellite Research Facility, MANA, International Center for Materials Nanoarchitectonics, National Institute for Materials Science
1–1 Namiki, Tsukuba, 305–0044, Japan

DOI: 10.1002/adfm.201303659

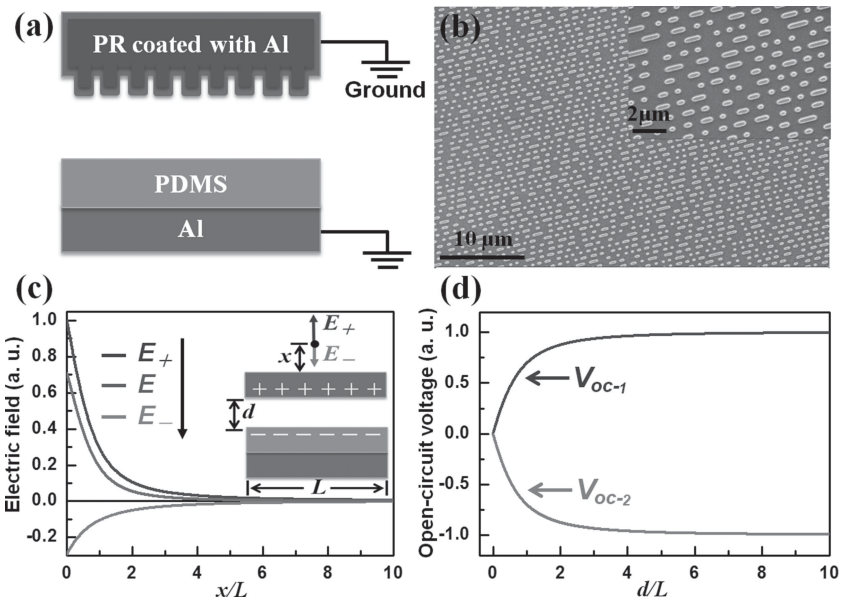

Figure 1. a) The structure diagram of the TENG. b) The SEM image of the Al film deposited on the PR sheet. c) The dependences of the calculated electric field at the points on the midperpendicular of the plates on x/L as $d = L$, the inset shows the diagram of the generated electric field. d) The dependences of the calculated open-circuit voltage-to-ground of the two-channel TEG-TENG on d/L.

with nanoscale protuberance structures was peeled from a commercial DVD disk to serve as the substrate, and then a 100-nm-thick Al film was deposited on the PR sheet to serve as both the top contact material and the top electrode. For the bottom plate, a 100-nm-thick Al film was deposited on a square Poly(methyl methacrylate) (PMMA) sheet to serve as the bottom electrode, and then a 100-μm-thick Polydimethylsiloxane (PDMS) layer was spin-coated on the bottom electrode to serve as bottom contact material. The SEM image of the Al film deposited on the PR sheet is shown in Figure 1b, which clearly shows the circular protuberances with a diameter of 300 nm and the rectangle protuberances with a width of 300 nm and a length of 800 nm. It is a low-cost and simple approach to construct the large-scale nanostructure by using the commercial DVD disk, which should largely simplify the fabrication processes and reduce the cost of the TENG. Both the nanostructure in the surface of the Al layer and the elastic property of the PDMS layer can increase the effective contact area of the two contact materials and enhance the electric output of the TENG.[21]

After the contact between Al and PDMS, the positive and negative tribo-charges are generated on the surface of Al and PDMS, respectively, due to their different triboelectric coefficients.[29–31] The open-circuit voltage-to-ground of the top and bottom electrodes ($V_{oc\text{-}1}$ and $V_{oc\text{-}2}$) are calculated using numerical simulation. As shown in the inset of Figure 1c, the total electric field (E) at a point x is superimposed by the positive electric field (E_+) caused by the positive charges on the Al surface and the negative electric field (E_-) caused by the negative charges on the PDMS surface. Here, we set $d = L$ (d is the separated distance between the two tribo-surfaces, and L is the side length of the square tribo-surfaces), and then the E, E_+, and E_- at various x points along the central axis of the tribo-surfaces are calculated, and their dependences on x/L are plotted in Figure 1c, in which the maximum electric field is normalized to 1. The $V_{oc\text{-}1}$ and $V_{oc\text{-}2}$ at a certain d value are calculated by integrating the curve of E from infinity to the top electrode and the bottom electrode, respectively. The dependences of $V_{oc\text{-}1}$ and $V_{oc\text{-}2}$ on d/L are plotted in Figure 1d, and the maximum voltage is normalized to 1. The curves of $V_{oc\text{-}1}$ and $V_{oc\text{-}2}$ are symmetric, in which they have similar absolute values and opposite polarities. The absolute values of $V_{oc\text{-}1}$ and $V_{oc\text{-}2}$ increase with d/L when d/L is lower than 2, and gradually reach saturation with the further increase of d/L, which is attributed to that the superimposed potential on top/bottom electrode by the charges on bottom/top plate decays with the increase of d.

The working mechanism of the two-channel TEG-TENG is shown in **Figure 2**. As shown in Figure 2a, the top and bottom electrodes are simultaneously grounded, and two electrical channels are formed. In the half cycle of separation, as the two tribo-surfaces are separated, the positive and negative voltage-to-ground are generated at the top and bottom electrodes, respectively, as a result, the positive and negative currents are generated and observed in channel 1 and channel 2, respectively (Figure 2b). As the separated distance d increases to its maximum value d' (2 cm in our experiment) and the electrical equilibrium is reached, $\sigma_{Al} \approx 0$ and $\sigma_{bott} \approx |\sigma_{PDMS}|$, as shown in Figure 2c. Here, σ_{Al}, σ_{PDMS}, and σ_{bott} are the charge densities on the Al tribo-surface, the PDMS tribo-surface, and the bottom

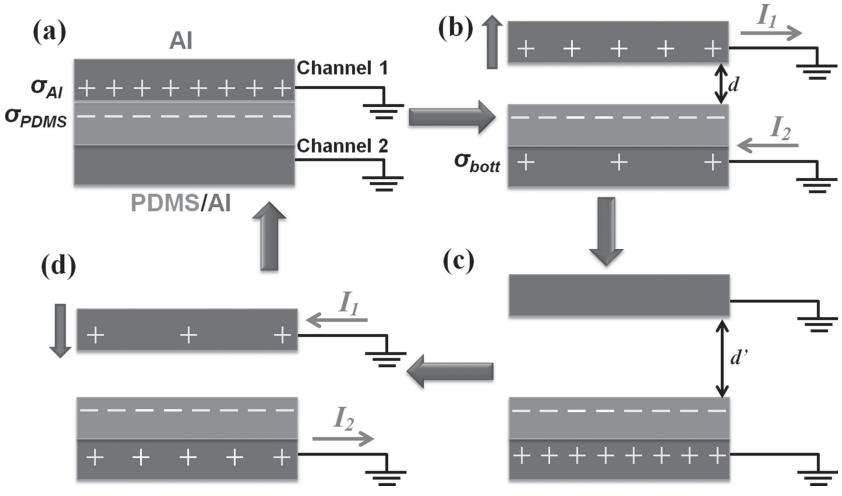

Figure 2. The working mechanism of the two-channel TEG-TENG.

DOI: 10.1002/adfm.201303659

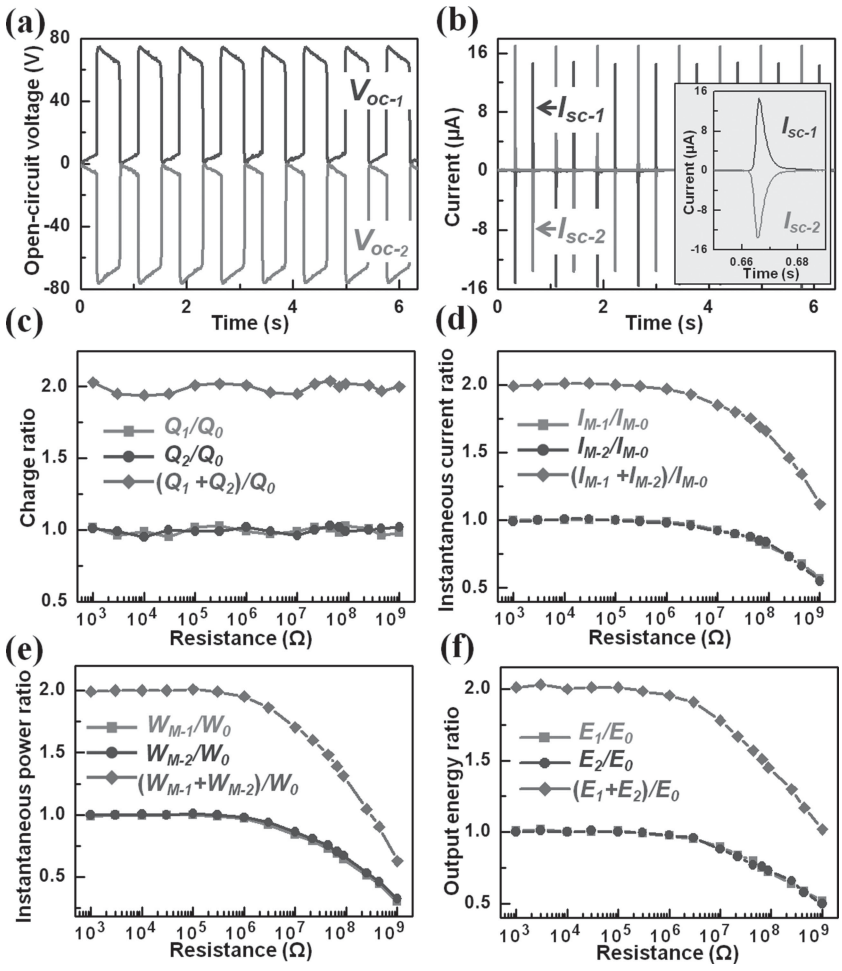

Figure 3. The a) open-circuit voltage and b) short-circuit current of the two-channel TEG-TENG. The dependences of c) the ratio of the absolute quantity of the flowed charges in a half cycle, d) the instantaneous maximum absolute current, e) the instantaneous maximum power, and f) the output energy in a total cycle between the two-channel TEG-TENG and the ungrounded TENG.

electrode, respectively. In the half cycle of contact, the top plate begins to move downward, and the negative and positive currents are generated and observed in channel 1 and channel 2, respectively, due to the negative and positive voltage-to-ground of the top and bottom electrodes respectively (Figure 2d). When the two tribo-surfaces are contacted, the electrical equilibrium is reached, in which $\sigma_{Al} = |\sigma_{PDMS}|$ and $\sigma_{bott} = 0$, as shown in Figure 2a. After that, the top plate moves upward again, and another cycle starts. The configuration of the two grounded electrodes can also be applied to other TENG modes, such as sliding and rotation disk modes, by connecting their two electrodes to the grounded.

In order to measure the electrical outputs of the two-channel TEG-TENG, two voltage or current meters were connected as two separated measurement systems to simultaneously measure the voltage or current from the two channels. The curves of open-circuit voltage-to-ground (V_{oc-1} and V_{oc-2}) and short-circuit current-to-ground (I_{sc-1} and I_{sc-2}) are shown in **Figure 3**a,b, respectively, and the magnification of a single peak of the short-circuit current is shown in the inset of Figure 3b. The open-circuit voltage and the short-circuit current of the two channels are nearly symmetric with similar absolute values and opposite polarities, which agrees well with the symmetric properties of the calculated V_{oc-1} and V_{oc-2} displayed in Figure 1d. The open-circuit voltage and short-circuit current of the ungrounded TENG (V_{oc-0} and I_{sc-0}) using the same device were also measured, and the working mechanism and the measured curves are shown in Supporting Information Figures S1,S2. It is found that, from the comparison, the open-circuit voltage of the two-channel TEG-TENG (about 75 V) is smaller than that of the ungrounded TENG (about 232 V), which is attributed to the counteraction of the electric field caused by σ_{Al} and σ_{PDM} as shown in Figure 1c. While, the instantaneous maximum absolute values of I_{sc-1} and I_{sc-2} (about 16.5 μA) are similar with that of I_{sc-0}, which is attributed to that the current at lower load resistance R ($R = 0$ Ω for short-circuit current) is dominated by the contact/separation speed of the two tribo-surfaces.[26] If the load resistances in the two channels, R_1 and R_2, are different, the output current curves of the two channels could be asymmetric with different instantaneous maximum absolute values, as shown in Supporting Information Figure S3.

The output current at various R of the two-channel TEG-TENG were measured (set $R_1 = R_2 = R$), and the output parameters of the two channels were calculated, including the absolute values of the charges transported in a half cycle (Q_1 and Q_2, calculated by integrating a single current peak in a half cycle), the instantaneous maximum absolute current (I_{M-1} and I_{M-2}), the instantaneous maximum power (W_{M-1} and W_{M-2}, calculated as $W = I^2R$), and the output energy in a total cycle (E_1 and E_2, calculated by integrating I^2R in the duration time of a total contact-separation cycle). The corresponding parameters of the ungrounded TENG (Q_0, I_{M-0}, W_{M-0}, and E_0) were also calculated for comparison. The dependences of Q_0, I_{M-0}, W_{M-0}, and E_0 on R are shown in Supporting Information Figure S4, and the dependences of the ratios of the parameters between the two-channel TEG-TENG and the ungrounded TENG on R are shown in Figure 3c–f. As shown in Figure 3c, Q_1 and Q_2 are both nearly equal to Q_0 in the range from 1 kΩ to 1 GΩ, and the sum of them are nearly two times of Q_0, which indicates that the two-channel TEG-TENG can double the collected charges compared to the ungrounded TENG. As shown in Figure 3d, as R is lower than 1 MΩ, I_{M-1} and I_{M-2} are both nearly equal to I_{M-0}, and the sum of them is nearly two times of I_{M-0}. As R is higher than 1 MΩ, I_{M-1}/I_{M-0} and I_{M-2}/I_{M-0} are smaller than 1, and the ratios decrease with the increase of R and decrease to about 0.55 at a load of 1 GΩ. As shown in Figure 3e,f, the ratios of instantaneous maximum power and output energy have similar properties with that of instantaneous

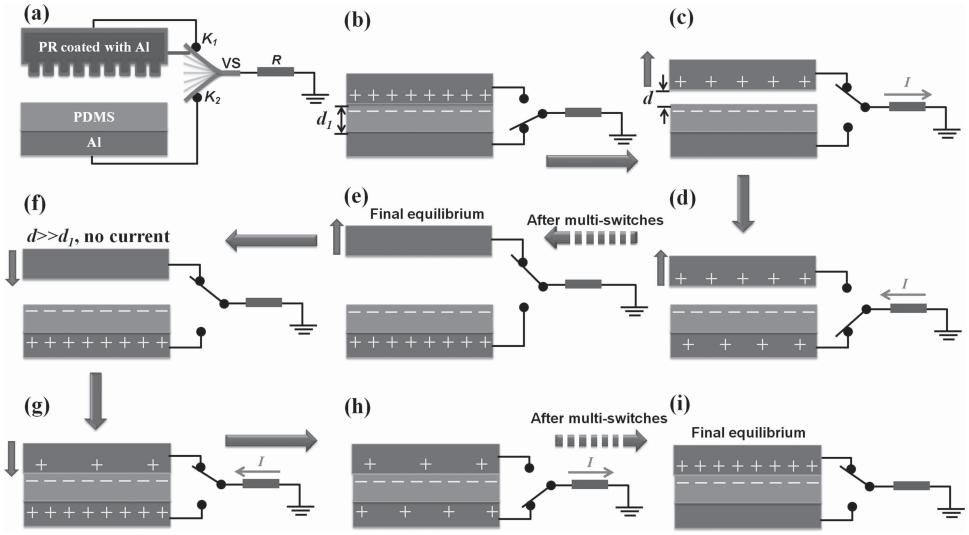

Figure 4. a) The structure diagram of the single-channel TEG-TENG with a self-triggered vibrating switch. The working mechanism of the single-channel TEG-TENG in b–e) the half cycle of separation and f–i) the half cycle of contact.

maximum current. These results indicate that, the two-channel TEG-TENG can provide twice the electric outputs compared to the ungrounded TENG as R is lower than 1 MΩ.

In order to collect the electric outputs of the TEG-TENG into a single closed circuit loop, the single-channel TEG-TENG with a self-triggered vibrating switch (VS) has been developed, which is schematically shown in **Figure 4**a. The top and bottom electrodes are connected to two metal contact points: K_1 and K_2. A vibrator made of rectangle stainless steel sheet is placed in the middle of K_1 and K_2 to perform as the VS, and one side of the VS is connected to the ground. An insulating object is fixed on the right side of the top plate to serve as a trigger of the vibrator, which impacts the edge of the VS with the motion of the top plate and triggers the vibrating of the VS. During the vibrating process, the VS is alternately switched to K_1 and K_2, as a result, the top and bottom electrodes are alternately connected to the ground to form an electrical channel. By accurately adjusting the positions of the VS, K_1, K_2, and the trigger, the VS can keep vibrating during the whole motion.

The working mechanism of the single-channel TEG-TENG is shown in Figure 4b–i. At initial stage (Figure 4b), the two tribo-surfaces are contacted and $\sigma_{Al} = |\sigma_{PDMS}|$, as a result, the voltage-to-ground of the top and bottom electrodes, V_1 and V_2, are both nearly zero. In the half cycle of separation (the top plate moves upward), as the VS is switched to K_1, the electrical channel between the top electrode and the ground is formed, and positive current is generated in this channel by the positive V_1, as a result, σ_{Al} decreases until V_1 is zero (Figure 4b). Due to the presence of negative potential caused by the negative charges on the bottom plate, σ_{Al} cannot decease to zero as V_1 is zero. Consequently, the VS is switched to K_2, and the negative current is generated in the electrical channel between the bottom electrode and the ground by the negative V_2, which leads to the increase of σ_{bott} until V_2 is zero (Figure 4d). For similar reason, $\sigma_{bott} < |\sigma_{PDMS}|$ as V_2 is zero. When the VS is switched to K_1 again, a positive V_1 appears again due to the positive potential caused by the increased σ_{bott}. Then, as the VS is alternately switched to K_1 and K_2, the positive and negative current is alternately generated, until the final electrical equilibrium is reached, in which $\sigma_{Al} \approx 0$ and $\sigma_{bott} \approx |\sigma_{PDMS}|$ (Figure 4e). In the half cycle of contact (the top plate moves downward), as the distance between the two tribo-surfaces (d) is much larger than the thickness of the PDMS layer (d_1, about 100 μm in our experiment), V_1 is nearly zero, and no current is generated, since V_1 is superimposed by the potential caused by σ_{PDMS} and σ_{bott} with distance of d_1 (Figure 4f). When the two tribo-surfaces are contacted or $d < d_1$, the negative and positive current are alternately generated as the VS is alternately switch to K_1 and K_2, respectively, as shown in Figure 4g,h. After multiple switching cycles, the final electrical equilibrium is reached, in which negative and positive current are alternately generated $\sigma_{Al} = |\sigma_{PDMS}|$ and $\sigma_{bott} = 0$ (Figure 4i).

Figure 5a shows the output current of the single-channel TEG-TENG at a load resistance of 2 MΩ and a motion triggering frequency of 2 Hz, and Figure 5b shows the magnification of the curve in a single cycle, in which multiple current peaks appear in each half cycle. In the half cycle of contact, the current curve consists of more than 20 current peaks, the positive and negative peaks alternately appear, and the absolute values of the peaks gradually decrease to zero. Similarly, in the half cycle of separation, about 7 positive and negative current peaks alternately appear, and the absolute peak value is higher than that in the half cycle of contact. As shown in Figure 5b, the interval time between two peaks with same polarity is 0.02 s, which corresponds to an output frequency of 50 Hz. The output frequency is determined by the resonant frequency of the VS (f_v), which is controlled by its length (L). The dependence of the output frequency on $1/L$ is shown in Figure 5c, and the output frequency increases linearly from 25 to 50 Hz as $1/L$ increases from 0.125 to 0.25 cm^{-1}. The linear dependence makes it simple to modulate the output frequency of the single-channel TEG-TENG. For The maximum peak

Adv. Funct. Mater. **2014**,
DOI: 10.1002/adfm.201303659

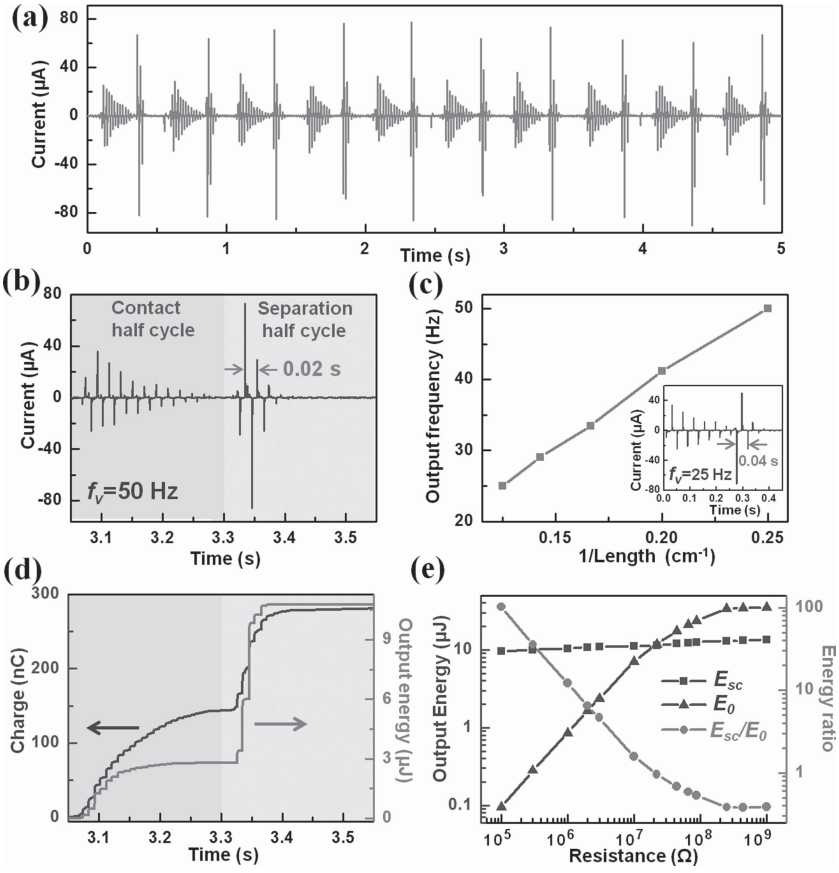

Figure 5. a) The output current curve with multiple cycles at a load resistance of 2 MΩ of the single-channel TEG-TENG with an output frequency of 50 Hz and a motion triggering frequency of 2 Hz. b) The magnification of the output current curve in a single cycle. c) The dependence of the output frequency on 1/*L*, and the inset shows the output current curve at a load resistance of 2 MΩ with an output frequency of 25 Hz. d) The curves of the absolute quantity of the flowed charges and the output energy in a single cycle. e) The dependences of E_{sc}, E_0, and E_{sc}/E_0 on the load resistance.

number in a half cycle is limited by f_v/f_{TENG}, where f_{TENG} is the motion triggering frequency of the TENG. As shown in Figure 5b, the final electrical equilibrium of the half cycle of contact is reached over 20 current peaks, which means that f_v is required to be higher than $20f_{TENG}$ to reach the final equilibrium. The output current curve at a load resistance of 2 MΩ as f_v being 25 Hz and f_{TENG} being 2 Hz is shown in the inset of Figure 5c, and only 12 current peaks appear in the half cycle of contact, which means that the final electrical equilibrium is not reached. Therefore, for TENG with higher motion frequency, it is necessary to increase f_v by decreasing the length of the VS.

By integrating the absolute value of the current curve in Figure 5b, the curve of the collected charge in a single cycle is obtained and shown in Figure 5d. The charge curve consists of many steps, and the difference value between the adjacent two steps corresponds to the charge transported during a single vibrating switch. The totally collected charges in the half cycle of contact and the half cycle of separation are 141 nC and 138 nC respectively, and both of them are about two times of the collected charges in a half cycle of the ungrounded TENG (about 71 nQ), which indicates that the single-channel TEG-TENG can also double the collected charges compared to the ungrounded TENG. By integrating I^2R using the current curve in Figure 5b, the curve of the output energy in a single cycle is obtained and shown in Figure 5d. Similarly, the output energy curve consists of many steps, and the difference value between the adjacent two steps corresponds to the output energy during a single vibrating switch. The total output energy in the half cycle of separation (8.0 μJ) is about 2.9 times of that in the half cycle of contact (2.8 μJ), and the maximum output energy during a single vibrating switch in the half cycle of separation (3.8 μJ) is about 5.4 times of that in the half cycle of contact (0.7 μJ). The higher output energy in the half cycle of separation is due to its higher voltage-to-ground values than the half cycle of contact.

By integrating I^2R using the current curves at various load resistance *R*, the output energies in a whole cycle of the single-channel TEG-TENG (E_{sc}) at various *R* are calculated, and the dependences of E_{sc}, E_0 (the output energy of the ungrounded TENG), and E_{sc}/E_0 on *R* are shown in Figure 5e. As *R* decreases from 1 GΩ to 100 kΩ, E_{sc} decreases from 13.5 to 9.6 μJ, E_0 decreases from 35.1 μJ to 94.3 nJ. In the range from 100 kΩ to 10 MΩ, E_{sc}/E_0 is higher than 1 and the ratio at 100 kΩ is 102, which indicates that the output energy of the single-channel TEG-TENG is largely enhanced at small load resistance compared to the ungrounded TENG. In the range from 22 MΩ to 1 GΩ, E_{sc}/E_0 is lower than 1 and the ratio at 1 GΩ is 0.38. For the ungrounded TENG with a lower *R*, more charges flow between the two electrodes in the initial stages of the contact/separation processes with lower output voltage, which decreases the total output energy in a single cycle. For the single-channel TEG-TENG, the top and bottom electrode are intermittently connected to the ground through the VS but not keep being connected to the ground, as a result, the flowed charges in the initial stages of the contact/separation processes are largely reduced, which increases the average potential of the total charges and the output energy in a single cycle at lower load resistance. While, for higher load resistance, only a small part of charges are flowed in the initial stages of the contact/separation processes for both the ungrounded TENG and the single-channel TEG-TENG, and the open-circuit voltage of the ungrounded TENG is higher than that of the TEG-TENG, therefore, the output energy of the single-channel TEG-TENG is reduced compared to the ungrounded TENG at higher load resistance.

In order to compare the performances of the single-channel TEG-TENG and the ungrounded TENG in practical applications, four green LEDs with total equivalent resistance of 100 kΩ are driven by these two types of TENGs through a full wave rectifying bridge. The motion frequencies of the TENGs

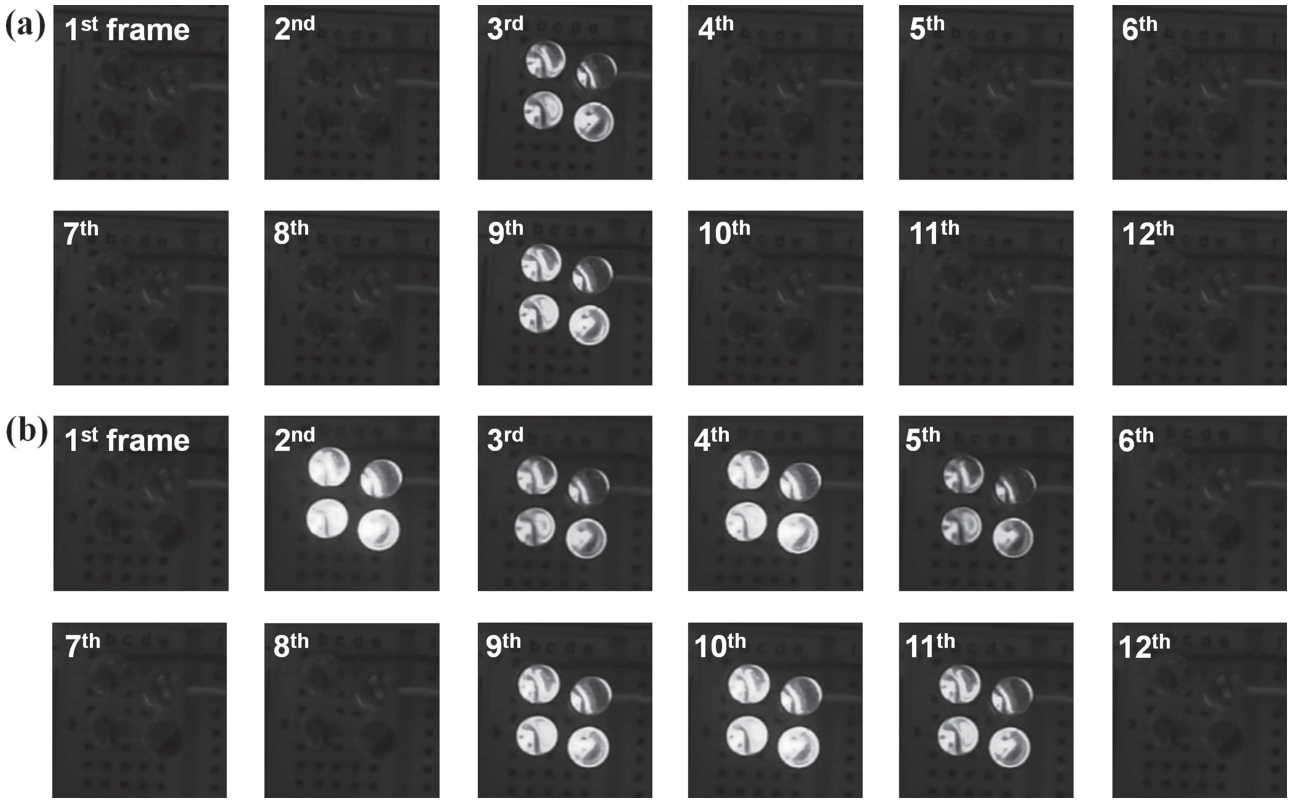

Figure 6. The pictures of the twelve frames in a single cycle as the LEDs are driven by a) the ungrounded TENG and b) the single-channel TEG-TENG at a motion frequency of 2 Hz.

are both 2 Hz, and the vibrating frequency of the single-channel TEG-TENG is 50 Hz. The videos of the emitted light of the LEDs were taken with a rate of 24 frames per second, and the pictures of all frames in a total cycle are shown in **Figure 6**. For the ungrounded TENG, the LEDs are only lighted in two frames (3rd and 9th frames), as shown in Figure 6a. For single-channel TEG-TENG, the LEDs are lighted in seven frames (2nd to 5th frames and 9th to 11th), as shown in Figure 6b. The higher number of the lighted frames comes from the longer duration time of the current peaks in the single-channel TEG-TENG as shown in Figure 5a. In addition, it is clear that the emitted light in the 2nd, 4th, 9th, and 10th frames of the single-channel TEG-TENG has higher brightness than that in the 3rd and 9th frames of the ungrounded TENG.

3. Conclusion

In summary, a two-electrode grounded (TEG)-TENG has been developed, in which the two electrodes are both grounded. Two modes of the TEG-TENG, two-channel mode and single-channel mode, have been demonstrated. For two-channel TEG-TENG, the two electrodes are simultaneously grounded to form two electrical channels with the ground, which can collect double charges, and provides double output energy at a load lower than 1 MΩ. For single-channel TEG-TENG, the two electrodes are alternately grounded through a self-triggered vibrating switch. About 30 current peaks with an output frequency of 50 Hz appear in a single cycle as the motion triggering frequency being 2 Hz, and the output frequency can be modulated from 25 to 50 Hz by adjusting the length of the vibrating switch. The output energy of the single-channel TEG-TENG is remarkably enhanced at a load lower than 10 MΩ compared to the ungrounded TENG, and the enhancing ratio is more than 100 at a load of 100 kΩ. As the LEDs are driven by the single-channel TEG-TENG, the lighted duration time is enhanced for about 3 times. The results indicate that the TEG-TENG is a new strategy for effective use of the energy harvested from our living environment.

4. Experimental Section

Fabrication of the TENG: First, the PR sheet was peeled from a commercial DVD disk to serve as the substrate of the top plate, and the PMMA sheet (thickness of 0.3 cm) was processed by laser cutting (PLS6.75, Universal Laser Systems) to serve as the substrate of the bottom plate. And then, the Al films of thickness of 100 nm were deposited on both the PR sheet and the PMMA sheet by e-beam evaporator. On the bottom plate, fluid PDMS that consists of base and curing agent in a ratio of 10:1 was spin-coated to form a 100-μm-thick layer. Then it was cured at 60 °C for 12 h. The contact area of the TENG is 4 cm^2.

Electric Output Measurement of TENG: In the electric output measurement, one plate was bonded onto a linear motor for the vertical contact-separation motion, the other plate was bonded onto a stationary XYZ linear translation stage. The current meter (SR570 low noise current amplifier, Stanford Research System) and voltage meter (6514 system

Adv. Funct. Mater. **2014**,
DOI: 10.1002/adfm.201303659

electrometer, Keithley) were used to measure the electric outputs of the TENGs.

Supporting Information

Supporting Information is available from the Wiley Online Library or from the author.

Acknowledgements

G.C. and Z.-H.L. contributed equaly to this work. This work was supported by MURI (Airforce Researcg Lab), Office of Basic Energy Sciences (DE-FG02–07ER46394), U.S. Department of Energy, NSF, NSFC (61176067), MANA, the World Premier International Research Center Initiative (WPI Initiative), MEXT, Japan, through a satellite lab at Georgia Tech. Patents have been filed based on the research presented here.

Received: November 27, 2013
Revised: November 20, 2013
Published online:

[1] Z. L. Wang, G. Zhu, Y. Yang, S. H. Wang, C. F. Pan, *Mater. Today* **2012**, *15*, 532.
[2] Z. L. Wang, W. Z. Wu, *Angew. Chem., Int. Ed.* **2012**, *51*, 11700.
[3] S. P. Beeby, M. J. Tudor, N. M. White, *Meas. Sci. Technol.* **2006**, *17*, R175.
[4] P. D. Mitcheson, E. M. Yeatman, G. K. Rao, A. S. Holmes, T. C. Green, *Proc. IEEE* **2008**, *96*, 1457.
[5] C. B. Williams, C. Shearwood, M. A. Harradine, P. H. Mellor, T. S. Birch, R. B. Yates, *Proc. IEEE Circ. Dev. Syst.* **2001**, *148*, 337.
[6] S. P. Beeby, R. N. Torah, M. J. Tudor, P. Glynne-Jones, T. O'Donnell, C. R. Saha, S. Roy, *J. Micromech. Microeng.* **2007**, *17*, 1257.
[7] P. D. Mitcheson, P. Miao, B. H. Stark, E. M. Yeatman, A. S. Holmes, T. C. Green, *Sens. Actuators A* **2004**, *115*, 523.
[8] Y. Naruse, N. Matsubara, K. Mabuchi, M. Izumi, S. Suzuki, *J. Micromech. Microeng.* **2009**, *19*, 094002.
[9] Z. L. Wang, J. H. Song, *Science* **2006**, *312*, 242.
[10] Y. Qin, X. D. Wang, Z. L. Wang, *Nature* **2008**, *451*, 809.
[11] C. E. Chang, V. H. Tran, J. B. Wang, Y. K. Fuh, L. W. Lin, *Nano Lett.* **2010**, *10*, 726.
[12] X. Chen, S. Y. Xu, N. Yao, Y. Shi, *Nano Lett.* **2010**, *10*, 2133.
[13] Y. F. Hu, L. Lin, Y. Zhang, Z. L. Wang, *Adv. Mater.* **2012**, *24*, 110.
[14] L. Gu, N. Y. Cui, L. Cheng, Q. Xu, S. Bai, M. M. Yuan, W. W. Wu, J. M. Liu, Y. Zhao, F. Ma, Y. Qin, Z. L. Wang, *Nano Lett.* **2013**, *13*, 91.
[15] K. I. Park, M. Lee, Y. Liu, S. Moon, G. T. Hwang, G. Zhu, J. E. Kim, S. O. Kim, D. K. Kim, Z. L. Wang, K. J. Lee, *Adv. Mater.* **2012**, *24*, 2999.
[16] F. R. Fan, Z. Q. Tian, Z. L. Wang, *Nano Energy* **2012**, *1*, 328.
[17] F. R. Fan, L. Lin, G. Zhu, W. Z. Wu, R. Zhang, Z. L. Wang, *Nano Lett.* **2012**, *12*, 3109.
[18] G. Zhu, C. F. Pan, W. X. Guo, C. Y. Chen, Y. S. Zhou, R. M. Yu, Z. L. Wang, *Nano Lett.* **2012**, *12*, 4960.
[19] S. H. Wang, L. Lin, Z. L. Wang, *Nano Lett.* **2012**, *12*, 6339.
[20] X. S. Zhang, M. D. Han, R. X. Wang, F. Y. Zhu, Z. H. Li, W. Wang, H. X. Zhang, *Nano Lett.* **2013**, *13*, 1168.
[21] G. Zhu, Z.-H. Lin, Q. S. Jing, P. Bai, C. F. Pan, Y. Yang, Y. S. Zhou, Z. L. Wang, *Nano Lett.* **2013**, *13*, 847.
[22] P. Bai, G. Zhu, Y. Liu, J. Chen, Q. S. Jing, W. Q. Yang, J. S. Ma, G. Zhang, Z. L. Wang, *ACS Nano* **2013**, *7*, 6361.
[23] S. H. Wang, L. Lin, Y. N. Xie, Q. S. Jing, S. M. Niu, Z. L. Wang, *Nano Lett.* **2013**, *13*, 2220.
[24] G. Zhu, J. Chen, Y. Liu, P. Bai, Y. S. Zhou, Q. S. Jing, C. F. Pan, Z. L. Wang, *Nano Lett.* **2013**, *13*, 2282.
[25] L. Lin, S. H. Wang, Y. N. Xie, Q. S. Jing, S. M. Niu, Y. F. Hu, Z. L. Wang, *Nano Lett.* **2013**, *13*, 2916.
[26] G. Cheng, Z.-H. Lin, L. Lin, Z. L. Du, Z. L. Wang, *ACS Nano* **2013**, *7*, 7383.
[27] Y. Yang, H. L. Zhang, J. Chen, Q. S. Jing, Y. S. Zhou, X. N. Wen, Z. L. Wang, *ACS Nano* **2013**, *7*, 7342.
[28] Y. Yang, H. L. Zhang, Z.-H. Lin, Y. S. Zhou, Q. S. Jing, Y. J. Su, J. Yang, J. Chen, C. G. Hu, Z. L. Wang, *ACS Nano* **2013**, *7*, 9213.
[29] G. S. P. Castle, *J. Electrostat.* **1997**, *40-41*, 13.
[30] L. S. McCarty, G. M. Whitesides, *Angew. Chem. Int. Ed.* **2008**, *47*, 2188.
[31] J. A. Wiles, B. A. Grzybowski, A. Winkleman, G. M. Whitesides, *Anal. Chem.* **2003**, *75*, 4859.
[32] Z.-H. Lin, G. Zhu, Y. S. Zhou, Y. Yang, P. Bai, J. Chen, Z. L. Wang, *Angew. Chem. Int. Ed.* **2013**, *52*, 5065.
[33] Z.-H. Lin, Y. N. Xie, Y. Yang, S. H. Wang, G. Zhu, Z. L. Wang, *ACS Nano* **2013**, *7*, 4554.
[34] Y. Yang, H. L. Zhang, Y. Liu, Z.-H. Lin, S. M. Lee, Z. Y. Lin, C. P. Wong, Z. L. Wang, *ACS Nano* **2013**, *7*, 2808.